JEE Journal of Ecological Engineering

Journal of Ecological Engineering, 2026, 27(9), 393–409
https://doi.org/10.12911/22998993/220576
ISSN 2299–8993, License CC-BY 4.0

Received: 2026.03.05
Accepted: 2026.07.15
Published: 2026.08.01

Spatiotemporal evolution of dissolved oxygen and hypoxia formation mechanisms in narrow-deep channel-type reservoirs: Insights from Shuikou Reservoir, China

Jin Chen[1], Chengchun Shi[1*], Jihui Liu[1], Yongshu Luo[2], Junhao Chen[2], Hui Li[2], Yang Qu[2]

[1] Fujian Provincial Key Laboratory of Environmental Engineering, Fujian Academy of Environmental Sciences, 350012 Fujian, China
[2] School of Ecological Environment and Urban Construction, Fujian University of Technology, 350000 Fujian, China
* Corresponding author's e-mail: fjhb-hky@sthjt.fujian.gov.cn

ABSTRACT

The dissolved oxygen (DO) dynamics in narrow-deep channel-type reservoirs under frequent hydrodynamic disturbances are distinct from those in conventional deep reservoirs. Through integrated monitoring of a representative reservoir in the Min River Basin, this study reveals that DO depletion results from the synergistic interaction of three mechanisms: thermal stratification, algal-nutrient feedback, and coupled topographic-circulation. It was found that a short-term yet thick thermocline (~20 m thickness, maximum ΔT 6.1 °C) serves as the primary physical barrier to vertical oxygen exchange, causing persistent bottom hypoxia (DO < 0.5 mg/L). High-frequency flood pulses (flushing rate α = 20.38) trigger abrupt mixing events, reducing vertical DO gradients by up to 79%. Algal photosynthesis leads to surface DO supersaturation (peak 9.1 mg/L), while algal sedimentation and decomposition, coupled with benthic ammonium release (0.32 mg/L), intensify bottom oxygen consumption. Furthermore, the channelized morphology near the dam (width-to-depth ratio 41.7) interacts with sluggish circulation to expand the hypoxic zone via horizontal advection, resulting in localized, year-round hypoxia. This study clarifies the DO evolution pathway under multi-mechanism synergy, providing a mechanistic basis for hypoxia prevention and ecological management in similar reservoirs.

Keywords: dissolved oxygen; thermal stratification; channel-type reservoir; hydrodynamic disturbances.

INTRODUCTION

Dissolved oxygen (DO) serves as a crucial indicator of aquatic ecosystem health, governing metabolic processes and exhibiting spatiotemporal patterns governed by the combined effects of physical mixing, biogeochemical processes, and human activities (Diaz and Rosenberg, 2008; Slavin et al., 2022). In deep reservoirs, hypolimnetic hypoxia resulting from persistent thermal stratification has been widely reported, with DO dynamics being closely related to thermocline stability and nutrient regeneration rates (Lembi, 2001; Wüest and Lorke, 2003). However, in narrow-deep channel-type reservoirs, characterized by frequent flood disturbances and short hydraulic retention times, the mechanisms driving DO depletion remain poorly understood, thereby significantly impeding effective ecological management (Morgenroth, 2019).

Narrow-deep channel reservoirs, mainly found in monsoon climates, have hydrodynamic behaviors that are quite different from conventional deep reservoirs. Intense flood pulses can cause sudden vertical mixing, and the channelized topography strengthens horizontal circulation, changing the material transport pathways (Keogh et al., 2019; van Heijst, 2014). Although it has been hypothesized that there are transitional states between stratification and mixing (North et al., 2014), there are still significant knowledge gaps in two aspects: the strength and duration of thermal stratification, and the efficiency of mixing events in oxygen replenishment (Caulfield, 2021; Kraemer et al., 2015).

In southeastern China, narrow-deep reservoirs are facing increasing hypoxia threats because of intensive aquaculture and extreme monsoon-driven rainfall. The Shuikou Reservoir in the Min River Basin is a typical example. Since 2004, it has experienced repeated hypolimnetic hypoxia (DO < 0.5 mg/L), which has led to massive fish kills in cage-culture zones (Zhang et al., 2022). Between 2016 and 2021, 27 disasters triggered by hypoxia were reported in this basin, causing economic losses of over 300 million CNY, and 83% of them were related to sudden DO drops. These crises highlight the urgent need to understand the mechanisms of hypoxia formation in such systems (Liu et al., 2019; Yan et al., 2021; Zhang et al., 2015).

This study looks into the Shuikou Reservoir by means of comprehensive hydrological and water quality monitoring from 2021 to 2022, aiming to answer two key questions about spatiotemporal DO variability as well as hypoxia formation mechanisms: (1) How do the dynamic thermal regimes, including short-term stratification and rapid mixing, affect the longitudinal (from headwater to dam) and vertical (from surface to bottom) DO gradients in different seasons? (2) What synergistic effects are there among thermal stratification, algal-nutrient interactions, and dam-proximal circulation in causing oxygen depletion and maintaining hypoxia hotspots? The findings will enhance the process-based management frameworks for DO restoration in subtropical channel reservoirs, thus supporting sustainable aquaculture and the protection of downstream water quality.

MATERIALS AND METHODS

Study area

The Shuikou Reservoir is located in the middle reaches of the Min River mainstream. It is a narrow-deep channel-type reservoir primarily for hydropower generation, with additional functions in navigation and flood control. The reservoir has a total storage capacity of 2.6×10^9 m^3, controls a drainage area of 52438 km^2, and spans approximately 106 km in channel length. The water surface area is 99.6 km^2, with an average width of 1 km (maximum 2.5 km) and water depths ranging 25～80 m (Figure 1).

The reservoir experiences a subtropical maritime monsoon climate, characterized by an annual average precipitation of 1500 mm and relative humidity of 77～86%. Since 2004, large-scale hypoxia events have frequently occurred in cage culture zones, resulting in massive fish mortalities and severe degradation of downstream aquatic ecosystems (Zhang et al., 2022).

Sampling sites and methods

Sampling sites

The study was conducted from September 2021 to July 2022, with seven sampling sections (S1–S7; Table 1, Figure 1) distributed along the longitudinal gradient of the reservoir. These sections included: S1, situated downstream of urban areas near an industrial zone and Liujia Village, experiencing frequent hydrodynamic disturbances; S2–S4 in transitional zones between rural and semi-urban areas, marked by significant tributary inflows, slow flow velocities, and intensive aquaculture activities; S5 and S6 adjacent to the dam backwater zone, exhibiting rapid flow regimes and strong turbulent mixing; and S7 located in the dam interception zone, characterized by pollutant accumulation and water depths exceeding 50 m.

Sampling methods

Sampling strictly followed the *Technical Specifications for Water Sample Preservation and Management* (HJ 493-2009, China). A 6-L stainless steel depth-stratified water sampler (WS-600; accuracy ±0.1 m) was used to collect water samples along left, middle, and right vertical transects of each section. Considering the pronounced longitudinal heterogeneity of the reservoir, sampling depths covered the surface layer (0.5 m), thermocline (10–25 m), and bottom layer (>30 m) to capture critical gradients of DO stratification.

Prior to sampling, the equipment was rinsed three times with in situ water. Surface water samples (0.5 m depth) were collected in duplicate (1000 mL per sample). Sample preservation followed these procedures: (1) Container pretreatment: Brown glass bottles were soaked in 1:9 (v/v) HCl for 24 h, sequentially rinsed with tap water and deionized water (three cycles each),

Table 1. Monitoring point information of Shuikou reservoir

Site	Name	Longitude (°E)	Latitude (°N)
S1	Liujia Bridge	118.4061	26.42098
S2	Downstream of Youxi Inlet	118.4794	26.39553
S3	Gutian Huangtian	118.5560	26.41841
S4	Lower Gutian Huangtian	118.6487	26.41845
S5	Wan Kou	118.6842	26.35668
S6	Minqing Xiongjiang	118.7484	26.34137
S7	Dam Front	118.7835	26.31429

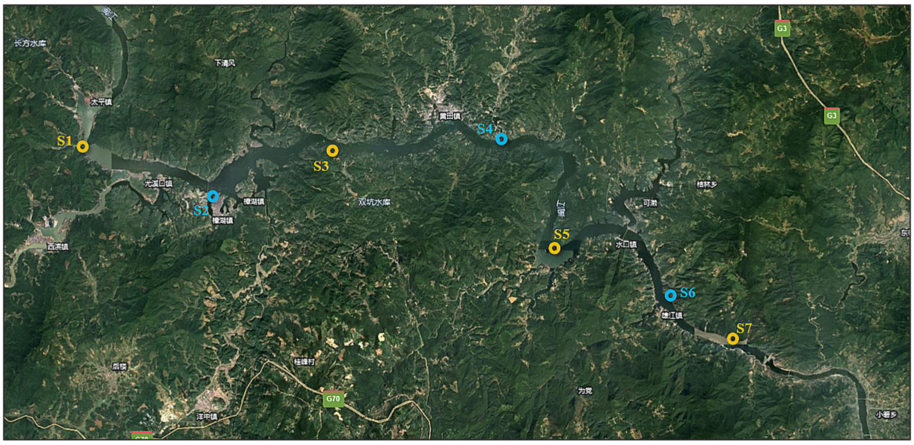

Figure 1. Hydrological and water environmental monitoring station location of Shuikou Reservoir

and oven-dried at 60 °C. (2) Sample fixation and storage: After adding preservatives, samples were stored in darkness at 4 °C, with laboratory analyses completed within 72 h.

Water quality measurements

Water quality parameters were measured through *in-situ* rapid detection and laboratory analyses. Field measurements employed a YSI Exo multiparameter water quality sonde to simultaneously record DO, water temperature (t), depth (h), chlorophyll a (Chl-a), pH, and conductivity. The instrument was lowered at a constant rate of 0.3 m/s, logging data every 0.5 s with a vertical resolution ≤0.1 m. Hydrological parameters, including flow rate, velocity, and cross-sectional area, were obtained using vessel-mounted acoustic Doppler current profiler (ADCP) surveys.

Laboratory analyses targeted total nitrogen (TN), total phosphorus (TP), ammonium (NH_3-N), nitrate (NO_3^--N), nitrite (NO_2^--N), and permanganate index, adhering to Chinese national standards: TN was analyzed via ultraviolet spectrophotometry (HJ/T 346-2007), NH_3-N using Nessler's reagent spectrophotometry (HJ 535-2009), and TP by ammonium molybdate spectrophotometry (GB 11893-1989). Quality control protocols incorporated blank tests and duplicate analyses, ensuring a relative deviation <5% across all procedures.

Data analysis

Thermal stratification was classified using three methodologies as follows (Gorham and Boyce, 1989; Lembi, 2001; Winton et al., 2019):

1) The α-β discrimination method calculated α as the ratio of inflow runoff (Q, m^3/s) to reservoir capacity (V, m^3), where α <10 indicates stable stratification, 10 ≤ α ≤20 denotes unstable stratification, and α >20 corresponds to fully mixed conditions. The β-index, defined as β = Qf/V (where Qf is flood discharge in m^3), further characterizes stratified reservoirs: β >1 suggests transient mixing during floods, while β <0.5 implies negligible flood impacts on thermal structure.
2) For the width-depth ratio method, the ratio R = B/H (B: average surface width; H: mean water depth) was applied. Reservoirs with H>15 m and R>30 were classified as mixed-type,

whereas R≤30 indicated stratification.

3) The hydraulic retention time method evaluated tres = V/Q (Q: annual average discharge). Thresholds were set as tres<10 days (mixed-type), 10 ≤tres≤100 days (unstable stratification), and tres >100 days (stable stratification).

Thermocline and oxycline depths were identified based on vertical gradients: temperature gradients ≥0.15 °C/m defined the thermocline, and DO concentration gradients ≥0.2 mg/(L·m) delineated the oxycline.

Data processing utilized Excel 2013 for raw data organization, Origin 9.0 for graphical visualization, and SPSS 23.0 for Pearson correlation analysis between environmental variables.

RESULTS AND DISCUSSION

Spatiotemporal variations in water temperature

Thermal stratification, as a critical physical mechanism regulating material and energy transport in reservoirs, profoundly influences DO distribution, nutrient transport, and biogeochemical cycles. Based on field observations from September 2021 to July 2022 in the Shuikou Reservoir of the Min River, this study established seven monitoring sections along the longitudinal gradient (from the Youxi Inlet to the dam front) to systematically investigate spatiotemporal stratification patterns through seasonal vertical temperature profiling (Figure 2).

Seasonal evolution of thermal stratification

Shuikou Reservoir exhibited a monomictic stratification-mixing cycle, as defined by a vertical temperature gradient threshold of 0.15 °C/m (Table 2). Stratification developed annually from May to September (stratified period), transitioning to full-depth mixing between October and April (mixed period). The evolution of thermal stratification comprised two distinct phases with unique hydrodynamic and thermal characteristics.

During the stratified period (May–September), a surface thermocline initially formed at 1–2 m depth in May (thickness: 2–4 m; surface-bottom ΔT: 3.6 °C), progressing to a dual-thermocline structure by July with surface (1–2 m) and deep (36 m) layers (ΔT: 3.4 °C). Stratification intensified through September, reaching a maximum surface-bottom ΔT of 6.1 °C and thermocline descent to 20–25 m (Table 2). Notably, the stratified period in Shuikou Reservoir (May–September) was delayed by 3–4 months compared to Luoxi Reservoir (March–November) and Panjiakou Reservoir (April–November). This delay reflects its riverine reservoir attributes: flood season runoff (April–June) accounts for >50% of annual inflow, while frequent water exchange (t_{res} = 0.05 days; Table 3) suppressed prolonged stratification.

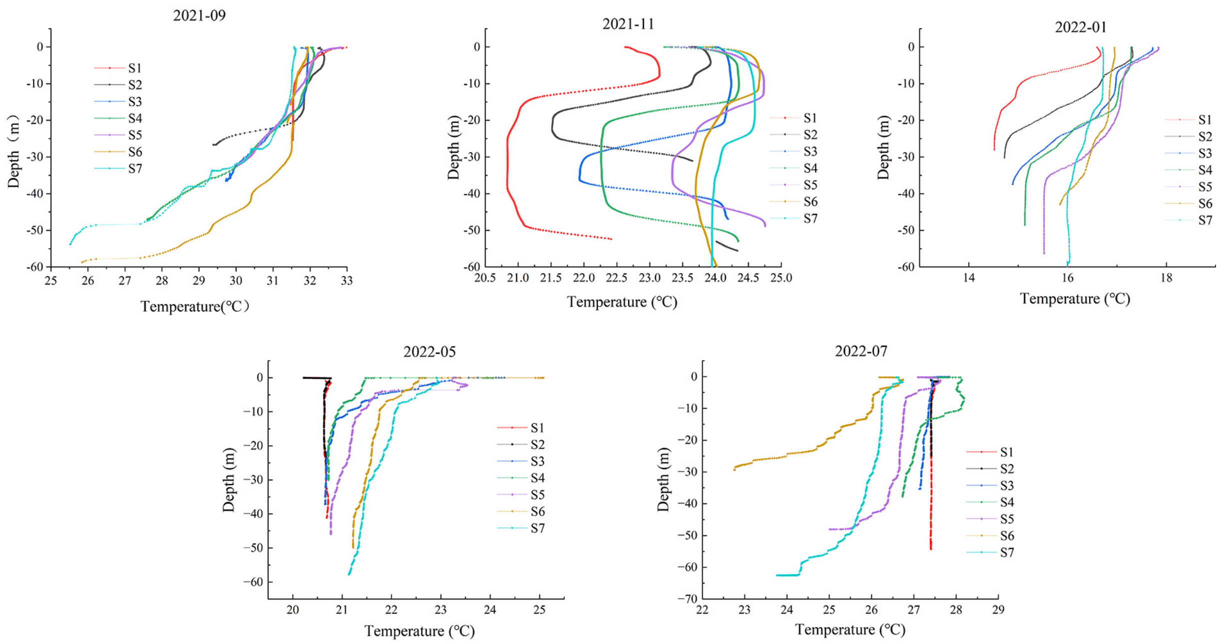

Figure 2. Spatiotemporal variations in vertical temperature distribution across different zones of Shuikou Reservoir (September 2021–July 2022)

The mixed period (October–April) commenced with declining air temperatures triggering vertical turnover in October, reducing the surface-bottom ΔT to 0.3 °C by November. However, a thermal anomaly occurred in January, with the surface-bottom ΔT rebounding to 2.4 °C and bottom water temperature (16.0 °C) becoming markedly lower than mid-depth layers (18.1 °C). This muted mixing pattern contrasts sharply with deep reservoirs like Qiandao Lake, which exhibit intense vertical overturn. The weaker thermal gradients in Shuikou Reservoir (maximum ΔT = 6.1 °C) accelerated mixing rates relative to strongly stratified systems, aligning with the rapid mixing mechanism in low thermal-gradient reservoirs.

Spatial temperature gradient variations

The spatial temperature distribution in Shuikou Reservoir is jointly controlled by topographic and hydrological conditions. Monitoring data from seven cross-sections along the reservoir axis (from the tail to the dam front) revealed pronounced spatial gradient patterns (Figure 2).

Longitudinal temperature gradients exhibited distinct seasonal dynamics. During the warming period (May–July), the temperature difference between the reservoir tail and dam front increased from 0.6 °C (May) to 2.8 °C (July), forming a downstream-warming gradient. This pattern resembled the summer stratification mode observed in Panjiakou Reservoir, though with weaker intensity (maximum ΔT: 5.2 °C in Panjiakou vs. 2.8 °C in Shuikou), primarily due to enhanced vertical mixing driven by high flood-season runoff (April–June accounting for >50% of annual inflow) (Gao Rui et al., 2022). During the cooling period (September–January), an upstream-cooling gradient emerged (ΔT = 2.8 °C), consistent with the “cold interflow” theory, where hypolimnetic inflows plunge to mid-depths (15–20 m), accelerating cooling in upper reaches(Çokacar, 2024). The mixing period (March–May) showed minimal thermal heterogeneity (ΔT≤1.1 °C, e.g., 0.6 °C in May), reflecting intermittent mixing typical of seasonally regulated reservoirs.

Vertical thermal stratification displayed pronounced seasonal variability. During the stratified period (July–September), a subdued surface thermal gradient (0.14 °C/m at 0–5 m depth, below the 0.20 °C/m thermocline threshold) coexisted with intensified subsurface stratification (0.25 °C/m at 20–25 m), matching the “bottom-enhanced stratification” mechanism in fluvial reservoirs (Okkonen and Kløve, 2010). The cooling transition phase (November) exhibited a sharp 2.0 °C thermal discontinuity at 15 m depth, corresponding to a 30% temperature decline relative to adjacent layers, signaling vertical penetration of cold interflow. Subsequently, the cold accumulation period (January) revealed a 1.5–2.0 °C thermal depression in bottom waters (>30 m), analogous to Qiandao Lake’s “bottom cold pool” paradigm but operating at reduced spatial scales (5–8 m thickness vs. 15–20 m in Qiandao Lake), demonstrating topography-modulated stratification dynamics(Han Xiaoxia et al., 2013).

Spatiotemporal heterogeneity of DO

The DO distribution in Shuikou Reservoir exhibited marked spatiotemporal heterogeneity, with vertical profile dynamics from September 2021 to July 2022 shown in Figure 3.

Seasonal stratification of DO

Vertical DO stratification displayed strong seasonal patterns coupled with thermal processes. During the stratified period (May–September), a stable thermocline (2–3 m thickness) at 10–15 m depth drove steep DO gradients. In September, surface DO (0–5 m) averaged 6.8 mg/L, decreasing to 3.2 mg/L at mid-depths (15–20 m) and plummeting to 0.5 mg/L in bottom waters (>30 m). Hypoxic conditions occupied ~52% of the total

Table 2. Thermocline parameters in Shuikou Reservoir

Time	Thermocline depth (m)	Thickness (m)	Surface-bottom temperature difference (℃)
September 2021	20–25	20 m to bottom	6.1
Time	Thermocline depth (m)	Thickness (m)	Surface-bottom temperature difference (℃)
November 2021	10–26	5–10	0.3
January 2022	3–20	6–14	2.4
May 2022	1–2	2–4	3.6
July 2022	1–2 m & 36 m (dual thermocline)	4–5 m & 36 m to bottom	3.4

water volume in this phase, resembling the strong stratification mode of the Three Gorges Reservoir, though Shuikou exhibited a thinner thermocline and higher vertical DO attenuation rates (Qiu et al., 2025). Diurnal variability peaked during stratification: daytime photosynthesis elevated surface DO to 9.1 mg/L (supersaturation), while nocturnal respiration reduced bottom DO to 0.3 mg/L.

During the mixed period (November–March), enhanced vertical mixing homogenized DO concentrations, reducing the surface-bottom difference from 6.3 mg/L (stratified phase) to 1.2 mg/L (January). However, localized hypoxia persisted in the deep channel near the dam, indicating incomplete mixing. This pattern aligned with winter mixing characteristics of Miyun Reservoir [4], but hypoxia duration extended by 15 days in Shuikou due to greater maximum depth (>56 m). Diurnal DO fluctuations decreased significantly (0.8 mg/L), reflecting hydrodynamic regulation of oxygen distribution.

Spatial gradient variation of DO

Longitudinal DO gradients exhibited a triphasic "high-low-extremely low" pattern from the reservoir tail to the dam. At the Liujia Bridge section (12 km upstream from the dam, reservoir tail), rapid flow velocity and strong reaeration capacity maintained a mean DO of 7.2 mg/L. Mid-reservoir conditions at the Gutian Huangtian section (6 km upstream) showed reduced DO (4.8 mg/L), while the dam-front Wan-kou section (1.5 km upstream) experienced further DO decline to 3.1 mg/L due to circulation stagnation effects. This longitudinal attenuation gradient aligns with typical riverine reservoir patterns, though Shuikou Reservoir's abrupt bathymetric increase near the dam drove a higher longitudinal DO attenuation rate (0.42 mg/(L·km)) compared to Danjiangkou Reservoir (0.25 mg/(L·km)) (Nong et al., 2024).

Coupling mechanisms of thermal stratification and DO dynamics

Stability discrimination and driving factors of thermal stratification

Shuikou Reservoir's thermal stratification exhibited dynamic short-term stratification and rapid mixing cycles. As determined by discriminant analysis (Table 3), this periodic variability results from synergistic interactions among hydrological perturbations, topographic constraints, and thermodynamic responses: (1) High-frequency flood disturbances dominated ephemeral stratification breakdown, with annual flood discharge averaging 9.22 × 10^8 m^3 (single-event range: 3–8.09 × 10^8 m^3). For instance, the 2010 flood event (8.09 × 10^8 m^3) abruptly reduced surface-bottom temperature differences from 5.8 °C to 1.2 °C, validating "flood-dominated stratification collapse" theory (Baker et al., 2021). The high runoff-storage ratio (α = 20.38) suppressed re-stratification,

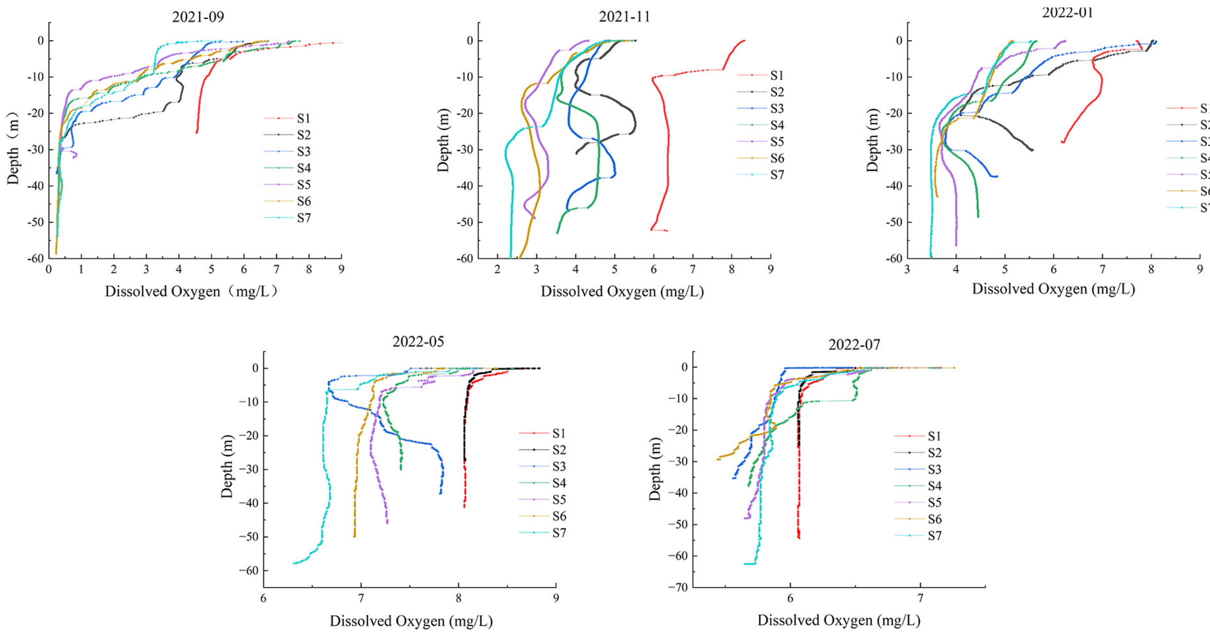

Figure 3. Vertical distribution and spatiotemporal variations of DO in different zones of Shuikou Reservoir (September 2021–July 2022)

Table 3. Stability evaluation of thermal stratification in Shuikou Reservoir

Analytical method	Formula	Key parameters	Criterion	Result	Conclusion
α-β criterion	$\alpha = Q/V$	Annual inflow: 53 billion m³; Capacity: 2.6 billion m³	$\alpha > 20$ indicates mixed regime	α=20.38	Critical mixed regime, highly unstable stratification
Analytical method	Formula	Key parameters	Criterion	Result	Conclusion
Width-depth ratio criterion	$R = B/H$	Mean river width: 1 km; Mean depth: 24 m	$R > 30$ indicates mixed regime	R=41.7	Fluvial topography suppresses vertical stratification
Hydraulic retention time method	$t_{res}=V/Q$	Capacity: 2.6 billion m³; Annual inflow: 53 billion m³	$t_{res}<10$ days indicates mixed regime	t_{res}=0.05 *yr*	Strong mixing dominates, short stratification periods

shortening recovery time by ~50% compared to Panjiakou Reservoir (Gao Rui et al., 2022). (2) Riverine geomorphic characteristics (width-depth ratio R= 41.7) and critical mixing parameters (α = 20.38) jointly constrain persistent stratification formation, contrasting sharply with lacustrine Dianchi Reservoir (R = 12) (Luo et al., 2018). (3) Thermodynamic feedbacks (maximum ΔT = 6.1 °C, vertical diffusion coefficient ≈ 0.12 cm²/s) accelerated stratification collapse by reducing mixing energy demand. These tripartite drivers collectively shape the reservoir's unique short-stratification/rapid-mixing regime.

Dynamics of thermal stratification stability and impacts

The stratification stability coefficient, defined as the ratio of surface layer thickness (Z_e) to maximum reservoir depth (Z_{max}), inversely correlates with stratification stability. A ratio <0.5 indicates stable stratification.

As shown in Table 4, the stability coefficient exhibited pronounced spatiotemporal heterogeneity linked to thermocline characteristics. During the stratified period (May–July), a thin epilimnion (Z_e≈2 m, Z_e/Z_{max}=0.034) intensified hypolimnetic oxygen depletion (rate: 0.24 mg L⁻¹ m⁻¹) through thermocline isolation. In the transition period (September), the stability coefficient increased to 0.34, accompanied by a thickened thermocline (20 m) and reduced thermal gradient (ΔT = 2.1 °C). By the mixed period (November), complete vertical mixing (Z_e/Z_{max} ≈ 1) diminished the DO vertical gradient from 6.3 mg/L (stratified phase) to 1.2 mg/L. However, hypoxia persisted in the dam-front deep channel during mixing due to bathymetry-induced eddy stagnation, which impeded vertical oxygen transport. This aligns with the "topography-circulation coupled oxygen regulation" mechanism, where channelized morphology suppresses turbulent mixing and horizontal oxygen advection, perpetuating localized hypoxia(Zhang et al., 2019). The coexistence of basin-wide mixing homogenization and persistent local hypoxia reveals a spatial interplay between hydrodynamic processes and geomorphic constraints, underscoring the dominance of terrain-modulated oxygen dynamics.

Synergistic evolution mechanisms of thermal stratification and DO

1) Spatiotemporal evolution of vertical DO stratification – DO stratification in Shuikou Reservoir exhibited strong synergistic evolution with thermal stratification. In May, as thermal stratification initiated, vertical DO gradients emerged, with the mixed layer depth aligning with the epilimnion. By July, a well-developed thermocline (ΔT = 5.2 °C; Table 3) nested the DO stratification below its lower boundary,

Table 4. Thermal stratification characteristics of Shuikou Reservoir across distinct periods

Parameter	Stratified period (May–July)	Transition period (September)	Mixed period (October–April)
Stratification stability coefficient (Z_e/Z_{max})	0.034	0.34	≈1 (full mixing)
Thermocline characteristics	Thickness: 2 m; ΔT: 5.2 ℃	Thickness: 20 m; ΔT: 2.1 ℃	ΔT<0.5 ℃, well-mixed
DO vertical gradient (mg L⁻¹)	6.3 (surface-bottom gradient)	3.8	1.2
Bottom oxygen consumption rate	0.24 mg L⁻¹ m⁻¹	—	—

contrasting with typical lacustrine reservoirs where oxygen clines typically reside above thermoclines. In September, DO concentrations in the 0–20 m surface layer sharply declined from 6–8 mg/L to <1 mg/L, forming an oxygen cline within the epilimnion. By November, complete vertical mixing ($Z_e/Z_{max} \approx 1$) induced anomalous mid-depth thermoclines and oxygen clines, whose depths progressively decreased from the reservoir tail to the dam front. By January, resurgent temperature and DO differences between surface and bottom layers reflected weakened water exchange after winter overturn cessation.

2) Drivers of DO stratification – DO stratification was primarily governed by high oxygen consumption rates and mixing dynamics. Summer bottom water temperatures rose from 16 °C (January) to 25.5–29.6 °C (September), enhancing microbial respiration (30–45% increase per 4 °C rise (Yang et al., 2018)). Coupled with organic inputs from cage aquaculture and decomposition of sinking algal particles, this led to hypolimnetic DO depletion rates exceeding surface reoxygenation capacity. Although vertical DO gradients drastically decreased during November mixing (decreased from 6.3 to 1.2 mg/L), bathymetry-induced eddies sustained hypoxia in the dam-front deep channel.

3) Coupling effects of thermal stratification and DO – thermal stratification regulated DO distribution through physical isolation and metabolic intensification. During May–July stratification, the thermocline blocked vertical oxygen exchange, confining DO gradients to the hypolimnion. In September, an anomalous epilimnetic oxygen cline emerged as hypolimnetic oxygen demand outpaced reoxygenation. From October to April, post-overturn cooling (≈14 °C interflow intrusion along mid-depths) and surface reoxygenation dominance amplified DO differences. These findings demonstrate that DO evolution in Shuikou Reservoir results from synergistic interactions among thermal forcing, topographic constraints, and biogeochemical processes.

Regulatory roles of algae and nutrients on DO

Spatiotemporal characteristics of algal activity

Algal dynamics in Shuikou Reservoir exhibited marked seasonal and spatial heterogeneity. Temporally, chlorophyll-*a* (Chl-*a*) concentrations peaked in September 2021 (20.3 μg/L) and January 2022 (40.2 μg/L), while remaining below 4 μg/L during other monitoring periods (Figure 4). These peaks coincided with the stratified period (September) and early mixing phase (January), highlighting light-thermal conditions and hydrodynamic stability as critical drivers of algal proliferation. Vertically, Chl-*a* concentrations declined sharply with depth, with the 0–3 m layer accounting for ~75%

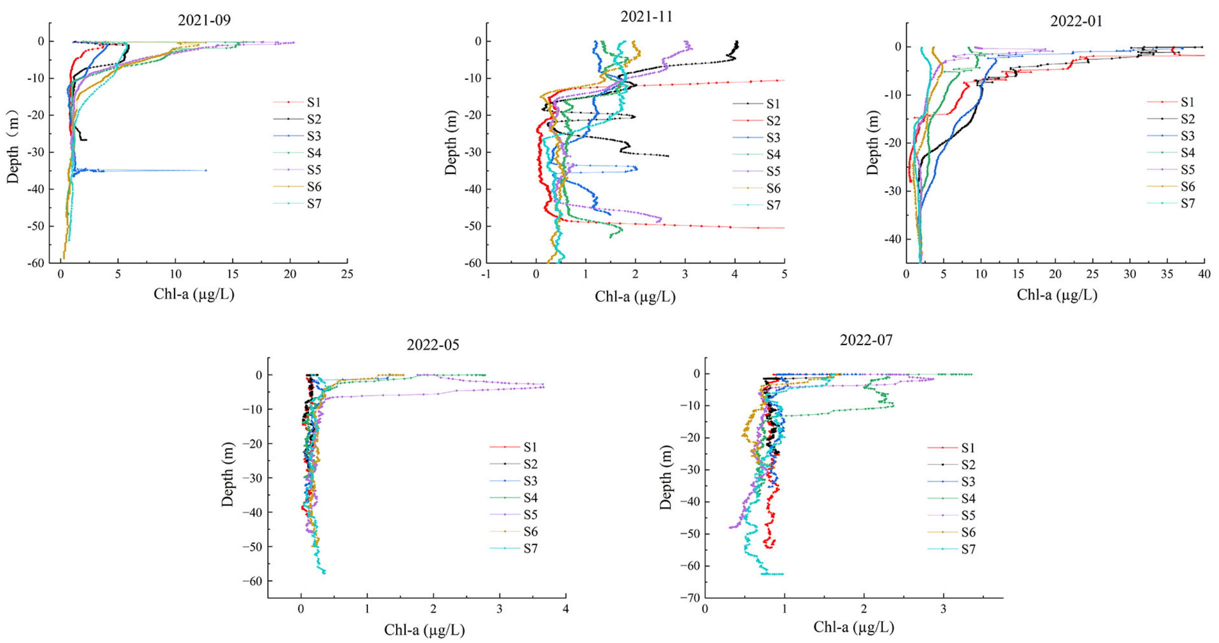

Figure 4. Spatiotemporal variations in vertical chlorophyll distribution across different zones of Shuikou Reservoir (September 2021–July 2022)

of total biomass (e.g., 20.3 μg/L at 3 m vs. <2 μg/L below 10 m in September). Spatially, Chl-*a* maximum were concentrated in mid-reservoir (Gutian Huangtian section: 20.3 μg/L) and near-dam areas (Wankou and Minqing Xiongjiang sections: 16.4 and 12.7 μg/L), contrasting with lower values at the reservoir tail (Liujia Bridge section: 5.1 μg/L). This spatial pattern underscores the preference of algal blooms for stagnant zones with reduced advective flushing.

Characteristics of nutrient distribution

Nutrients in Shuikou Reservoir exhibited pronounced spatiotemporal heterogeneity, with distinct concentration dynamics and exceedance risks across parameters (Figure 5). COD_{Mn} and TN followed synchronous trends, peaking in September 2021 and subsequently declining due to runoff dilution and biological uptake. However, TN consistently exceeded the Class III water quality standard (TN ≤1.0 mg L^{-1}) annually, indicating persistent exogenous nitrogen inputs (e.g., agricultural non-point sources, aquaculture feed).

NH_3-N and nitrite nitrogen NO_2^--N displayed bimodal seasonal fluctuations, peaking in summer-autumn and declining in winter-spring. NH_3-N peaked at 0.16 mg L^{-1} in May, driven by agricultural runoff during the early flood season (April–June) and sediment ammonification accelerated by rising temperatures. NO_2^--N peaked at

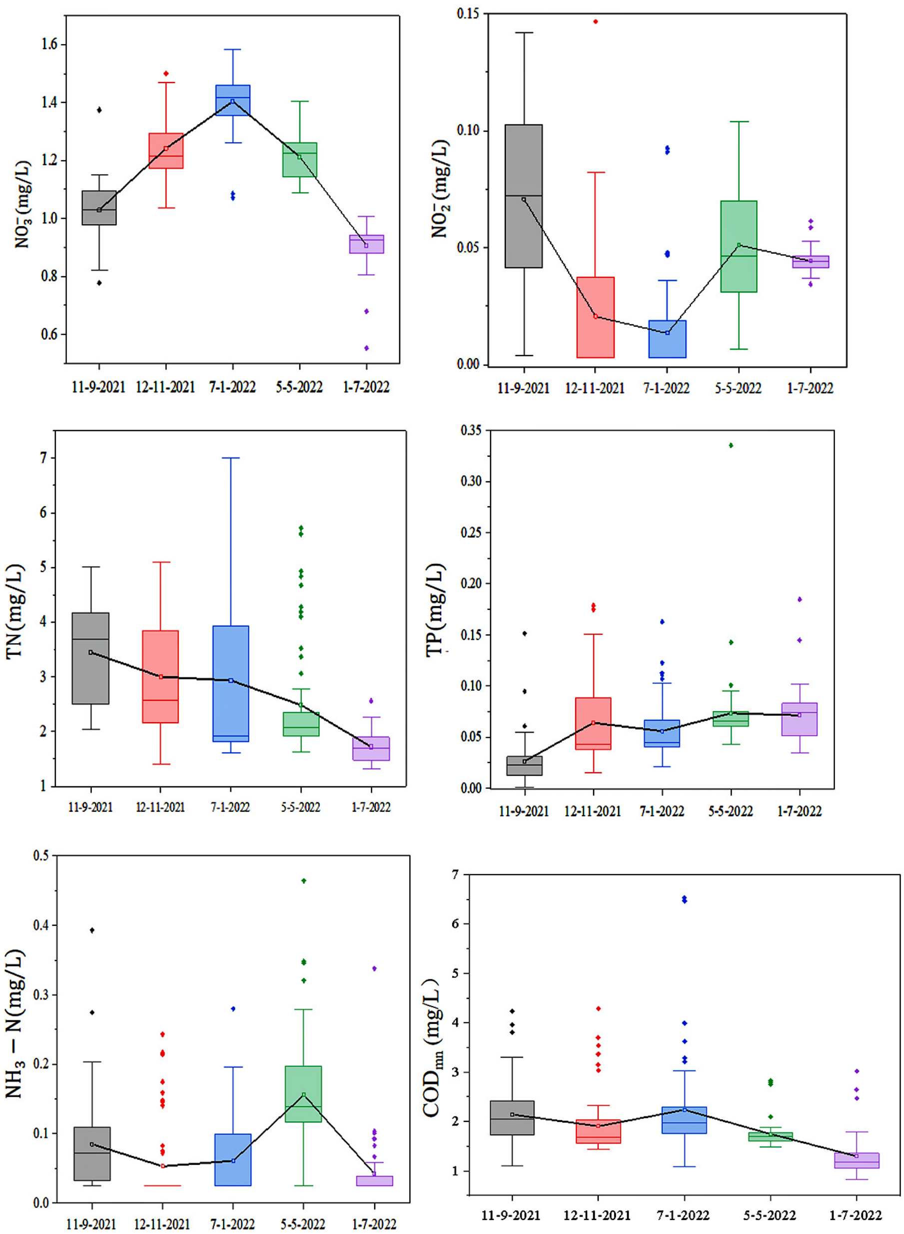

Figure 5. Temporal trends of nutrient parameters in Shuikou Reservoir (September 2021 – July 2022)

0.075 mg L^{-1} in September, linked to hypoxia-inhibited nitrite-oxidizing bacteria (NOB) activity under stratified conditions, stalling nitrification at the nitrite stage.

NO_3^--N concentrations peaked at 1.43 mg L^{-1} in January 2022, likely attributed to winter low temperatures suppressing denitrification and shortened hydraulic retention enhancing nitrogen retention. TP reached its minimum in September (0.024 mg L^{-1}) but surged to 0.071 mg L^{-1} by November (exceedance rate: 42%; Class III standard: TP ≤0.05 mg L^{-1}), highlighting sediment resuspension and exogenous inputs during mixing. These nutrient patterns interacted strongly with algal activity and oxygen stratification: high TN/TP loads in summer-autumn fueled algal blooms, while sediment ammonification and nitrification exacerbated hypolimnetic oxygen depletion.

Vertical profiles (data not shown) indicated that NH_3-N concentrations increased significantly with depth, exhibiting bottom concentrations (>30 m) approximately 1.8 times higher than surface levels. For instance, in September, surface waters measured 0.12 mg L^{-1} compared to 0.32 mg L^{-1} at depth. Similarly, TP followed an analogous distribution pattern, with bottom concentrations about 1.5 times greater than surface values (0.04 mg L^{-1} at the surface versus 0.06 mg L^{-1} in deeper layers during September). In contrast, COD_{Mn} displayed an inverse vertical trend, decreasing with depth; surface waters (0–5 m) registered 2.8 mg L^{-1}, while bottom concentrations reached 2.5 mg L^{-1} in the same month.

Interactive mechanisms of algae, nutrients and DO

Algal activity dynamically couples with nutrient and dissolved DO dynamics through metabolic processes, exhibiting bidirectional feedback regulated by thermal stratification. During positive driving phases, algal peaks (September and January) elevate surface DO via photosynthesis (e.g., 9.1 mg L^{-1} in September) while depleting NO_3^--N through uptake, creating synergistic surface oxygenation and nutrient competition. In negative feedback phases, sinking algal debris enhances hypolimnetic oxygen consumption via particulate organic carbon decomposition, while sediment-released NH_3-N further depletes DO through nitrification, coupling hypoxia with nitrogen cycling. This bidirectional interplay, combined with vertical DO gradients (surface-high, bottom-low;) and nutrient dynamics (e.g., 42% TP exceedance;), governs the equilibrium between self-purification and pollution accumulation.

Spatial heterogeneity amplifies regional divergences. In mid-reservoir zones (e.g., Gutian Huangtian section, flow velocity: 0.05–0.1 m s^{-1}), active flow synchronizes algal photosynthesis with DO elevation, enhancing nutrient uptake efficiency. Conversely, dam-front stagnant areas (>50 m depth, <0.05 m s^{-1}) experience intensified hypoxia (Figure 3) due to algal settling coupled with sediment NH_3-N release, reducing bottom DO recovery rates by ~60% compared to surface layers. This spatial variability synergizes with thermal gradients (e.g., bottom cold pools;) and longitudinal DO attenuation ().

Thermal stratification physically bridges these biogeochemical processes. Stratified-period thermoclines (20–25 m) block vertical mixing, preventing surface DO production from offsetting hypolimnetic consumption (bottom DO <2.0 mg L^{-1} in ~52% of cases). Mixing-period overturn promotes sediment resuspension (e.g., TP rising to 0.071 mg L^{-1}), seeding nutrients for subsequent algal blooms. This annual cycle underscores the deep coupling between thermodynamic processes and algae-nutrient-DO interactions.

Spatial linkage mechanisms between DO and environmental factors

Pearson correlation analyses of DO and environmental factors across seven monitoring sections (S1–S7) from the reservoir tail to the dam front revealed significant spatial heterogeneity in DO drivers, with distinct dominant processes across zones (Figure 6). In the tail zone (S1), DO dynamics were jointly regulated by thermal stratification and nitrification. A strong negative correlation between water temperature and DO (r = −0.585, p <0.01) indicated that the thermocline (20–25 m depth) exacerbated bottom hypoxia (DO<0.5 mg L^{-1}) by suppressing vertical mixing. Simultaneously, the significant negative correlation between NO_2^--N and DO (r = −0.731, p < 0.01) reflected nitrification inhibition under hypoxic conditions, as evidenced by elevated bottom NH_3-N concentrations (0.32 mg L^{-1} vs. surface 0.12 mg L^{-1}), consistent with sediment ammonification and nitrification-driven oxygen consumption during stratification.

Transitioning toward the mid-reservoir sections (S2–S4), algal activity emerged as a core regulator of DO. A highly significant positive correlation between Chl-*a* and DO at S3 (r = 0.658, p <0.01) confirmed the photosynthetic oxygenation effect in surface waters. The positive correlation between NO_3^--N and DO (r = 0.503, p <0.01) suggested either oxygen-rich inflows carrying nitrate or delayed algal nitrate uptake relative to oxygen production. Additionally, the significant positive correlation between TP and DO at S4 (r = 0.546, p <0.01) indicated synchronized phosphorus assimilation and photosynthetic DO elevation.

In the dam-front deep channel (S5–S7), hypoxia mechanisms shifted toward sediment disturbance and nitrogen cycling coupling. Strong negative correlations between conductivity and DO at S6 and S7 (r = −0.796 and −0.687, p <0.01) implicated oxygen depletion via ionic release (e.g., Fe^{2+} oxidation) during sediment resuspension. Notably, while TP exhibited a positive correlation with DO at S7 (r = 0.417, p <0.01), suggesting indirect DO enhancement through algal phosphorus uptake, NO_3^--N showed a negative correlation (r = −0.228, p < 0.05), implying enhanced denitrification under hypoxic conditions. This aligns with nitrate reduction to N_2O or N_2 in stagnant flow environments (velocity <0.05 m s^{-1}),.

Spatially, DO dynamics transitioned from physical isolation in upstream zones to algal metabolic control in mid-reservoir areas and sediment-driven hypoxia near the dam. Seasonal shifts in thermal stratification (stratified period: May–September; mixed period: October–April) further amplified this spatial heterogeneity, creating a continuum of biogeochemical interactions from reservoir tail to dam front.

Regulation of DO by hydrodynamic and circulation processes

Impacts of flow and water level variations on DO

Hydrological monitoring results for each section of Shuikou Reservoir during the experimental period (September 2021–July 2022) are shown in Table 5. At the reservoir tail (S1), flow rates sharply decreased from 567 m^3/s in September 2021 to 61 m^3/s in January 2022 (an 89% reduction), then rebounded to 2100 m^3/s in May 2022 and further increased to 2900 m^3/s by July 2022. Mainstream sections (e.g., S3) exhibited synchronized drastic fluctuations, with flows declining from 522 m^3/s in September 2021 to 402 m^3/s in January 2022, followed by a surge to 4040 v in July 2022 (~900% increase).

From November 2021 to January 2022, the dam-front sections displayed reverse flow characteristics: the average flow at S5 was -164 m^3/s, while S6 fluctuated between -522 m^3/s and 220 m^3/s. By July 2022, the dam-front S7 section recorded a flow rate of 3820 m^3/s, representing a 976% increase compared to January (m^3/s).

From September 2021 to July 2022, the dynamic regulation of dam discharge and dam-front water levels in Shuikou Reservoir exhibited significant spatiotemporal heterogeneity (Figure 7). The discharge-storage cycle was characterized by low discharge (300 m^3/s) and low water level (58.5 m) in September 2021, followed by a sharp surge in discharge to 3.000 m^3/s by May 2022, which lowered the water level to 59.34 m. This completed a discharge-storage-discharge cycle, accompanied by a distinct low-high-low water level fluctuation pattern.

Hydrodynamic processes modulated DO through three distinct phases: (1) Low-discharge, low-water-level phase (September 2021): Reduced dam-front flow velocity (~0.12 m^3/s at section S7) enhanced algal sedimentation (chlorophyll-*a* peaks: 18.6 μg/L), forming a high oxygen consumption zone in bottom waters (DO <0.5 mg/L); (2) High-discharge, low-water-level phase (May 2022): Discharge exceeding 3000 m^3/s elevated dam-front flow velocity (~0.35 m^3/s at S6), intensifying vertical mixing and

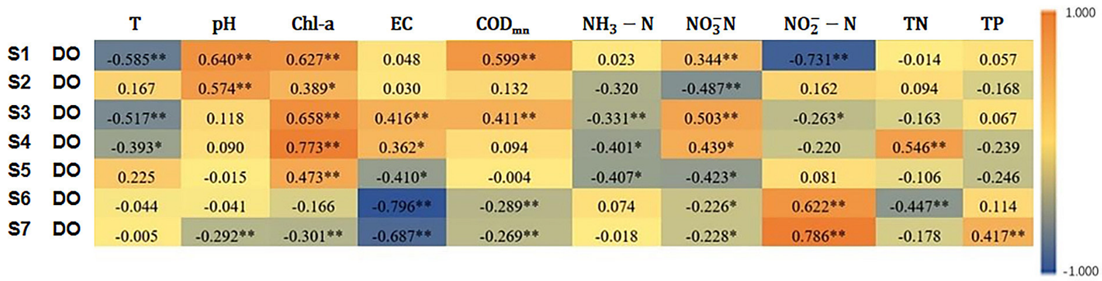

Figure 6. Heatmap of Pearson correlation analysis between DO and environmental factors across different zones of Shuikou Reservoir (* for $p < 0.05$ and ** for $p < 0.01$)

Table 5. Statistical results of hydrological monitoring in Shuikou reservoir (m^3/s) (September 2021–July 2022)

Section		Measurement Type	Sep. 2021	Nov. 2021	Jan. 2022	May 2022
S1	Forward	528	-136	-16	2120	2890
	Return	606	389	138	2080	2920
	Average	567	126	61.0	2100	2900
S2	Forward	500	42.8	456	2470	3370
	Return	533	121	512	2420	3540
	Average	516	81.9	484	2440	3460
S3	Forward	473	406	448	2900	4070
	Return	570	338	356	2670	4000
	Average	522	372	402	2780	4040
S4	Forward	613	170	160	2210	3510
	Return	519	69	-12	2390	3250
	Average	566	119	74	2300	3380
S5	Forward	442	-523	-194	2430	3570
	Return	478	-487	-135	2490	3570
	Average	460	-505	-164	2460	3570
S6	Forward	445	-391	164	2790	3560
	Return	467	-653	276	2830	3540
	Average	456	-522	220	2810	3550
S7	Forward	390	-443	259	2900	3990
	Return	45.4	260	451	3230	3640
	Average	218	-92	355	3060	3820

reducing the DO gradient from 6.3 mg/L (stratified period) to 1.2 mg/L. (3) High-water-level phase (November 2021–January 2022): Vertical shear flows in dam-front deep channels (coexisting negative flow at S5 and positive flow at S7) uplifted hypoxic bottom waters to mid-depths (15–20 m). Concurrently, enhanced inertial flows in the main channel under low-water conditions (59.34 m), with $Re > 8 \times 10^6$ (estimated for velocity 0.35 m/s and depth 24 m), disrupted thermocline stability, accelerating the recovery rate of bottom DO.

Transport mechanisms of hypoxic water by dam-front circulation

The dam-front circulation structure exhibited spatiotemporal heterogeneity with water level variations (Figures 8 and 9) and regulated the transport and retention of hypoxic water through three-dimensional hydrodynamic processes.

During the low-water-level period, the surface layer at section S6 exhibited distinct downstream flow in September 2021, while transverse flow components and reverse flow were observed in the surface layers of sections S5 and S7. Deep-layer velocity vectors displayed multidirectional distributions (Figure 8), indicating the coexistence of transverse and longitudinal circulation in the dam-front area, with the longitudinal circulation extending to section S6. By May 2022, the longitudinal circulation had nearly disappeared. At section S5, V-shaped channel topography induced flow deflection, generating transverse flow components and reverse flow in the surface layer, while the deep layer maintained downstream flow throughout. At section S4, both surface and bottom layers exhibited downstream flow, with localized surface reverse flows likely associated with wind-driven currents. During the high-water-level period, reverse flow dominated the surface layers from sections S2 to S7 in November 2022, while deep-layer velocity vectors showed three-dimensional divergence, expanding the influence of circulation to section S2 (Figure 9). By January 2022, surface flow velocities had weakened compared to November 2022, but the spatial coverage of circulation continued to expand.

Dam-front circulation directly shaped the spatiotemporal distribution of dissolved oxygen (DO) by regulating water transport pathways,

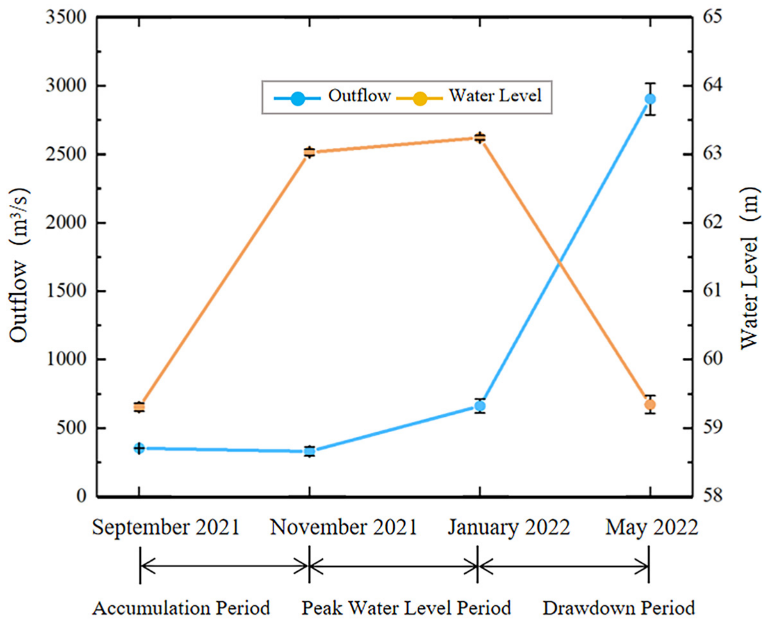

Figure 7. Mean flow rate (m^3/s) and mean dam-front water level (m) in the study area during the sampling period (September 2021–July 2022)

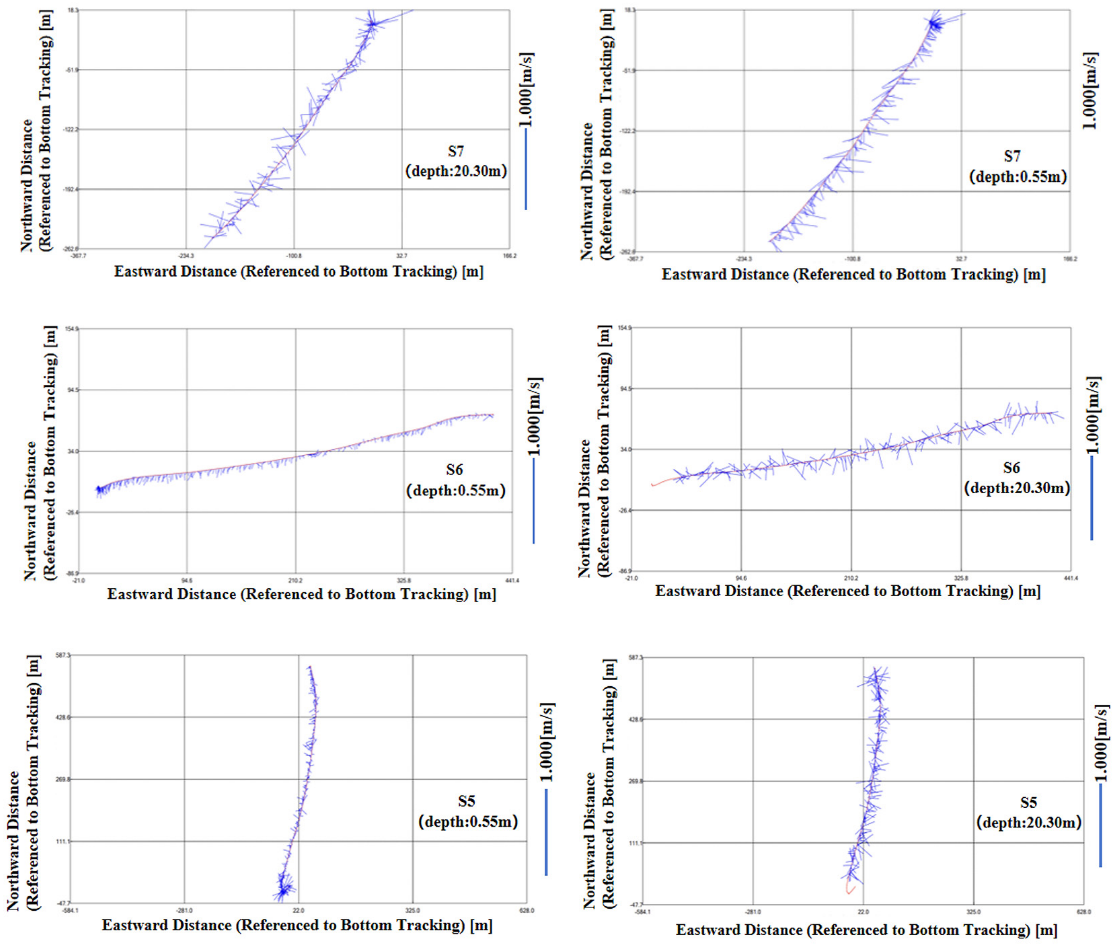

Figure 8. Velocity vector diagrams at typical depths (surface and bottom layers) along cross-sections during the low-water-level period (S7–S5 sections September 2021): Blue lines represent the collection trajectory of flow velocity vectors at the corresponding depth, and red line denotes the spatial boundary reference line of the S5 section

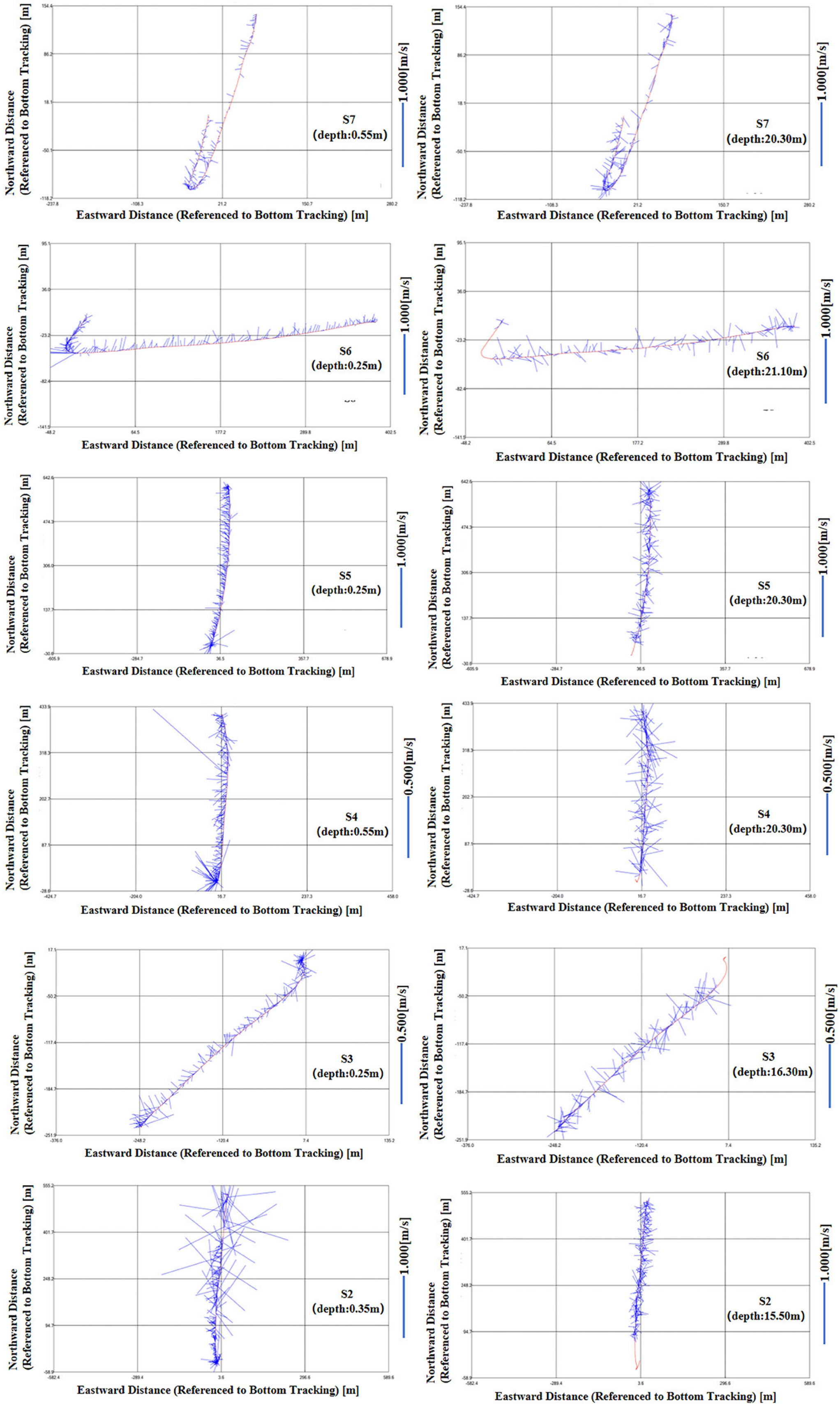

Figure 9. Velocity vector diagrams at typical depths (surface and bottom layers) along cross-sections during the high-water-level period (S7–S2 sections November 2021): Blue lines represent the collection trajectory of flow velocity vectors at the corresponding depth, and red line denotes the spatial boundary reference line of the S5 section

primarily through two key processes: vertical migration of hypoxic water and longitudinal diffusion of hypoxic water. The mechanisms and impacts of these processes are described as follows.

First, vertical migration of hypoxic water driven by circulation occurred during water storage periods. Inertia-driven longitudinal circulation (surface flow toward the dam and reverse bottom flow) transported hypoxic water from mid-lower layers to the surface, causing significant DO declines in surface waters (e.g., surface DO at S5 decreased from 6.8 mg/L to 4.2 mg/L). Concurrently, oxygen-rich inflow along the main channel temporarily elevated DO in localized bottom areas (e.g., bottom DO at S7 increased from 0.3 mg/L to 2.3 mg/L). This process resembles density-driven flow in deep reservoirs but accelerates hypoxic water diffusion due to the riverine morphology of Shuikou Reservoir (width-depth ratio of 41.7) and high-frequency disturbances (t_{res} = 0.05 years). Second, longitudinal diffusion of hypoxic water was exacerbated by circulation. During the October 2021 "fish mortality event", coupling of dam-front reverse flow (S5: -164 m^3/s) and topographic circulation transported hypoxic water from the Minqing Xiongjiang section (S6, 1.5 km upstream) to the central reservoir, reducing mid-layer DO at the Gutian Huangtian section (S3) to 0.8 mg/L. Monitoring revealed that bottom DO at the bay mouth (S5) plummeted to 0.5 mg/L (below the tolerance threshold of 4 mg/L for cyprinid fish), resulting in a 35% mortality rate in cage-cultured fish. During this period, DO levels <1.2 mg/L were widespread in the 0–30 m depth range from the central reservoir to the dam, while the reservoir tail (S1) maintained higher DO levels due to inflow reoxygenation, highlighting the spatial heterogeneity of hypoxia stress.

Drivers of low DO and mitigation strategies in Shuikou reservoir

Synergistic effects of multiple factors on low DO

The spatiotemporal heterogeneity of dissolved oxygen in Shuikou Reservoir is jointly influenced by thermal stratification, biogeochemical processes, and topographic circulation.

Thermal stratification dynamics dominate vertical oxygen transport. During the stratified period (May–September), the thermocline (thickness: 20 m; surface-bottom temperature difference: 6.1 °C) physically inhibits vertical mixing, causing persistent bottom hypoxia (DO <0.5 mg/L). High runoff-to-reservoir-capacity ratio (α = 20.38) and flood disturbances (e.g., July discharge: 4040 m^3/s) enhance vertical mixing, reducing the DO gradient by 79% (from 6.3 mg/L to 1.2 mg/L). Algal metabolism drives bidirectional DO feedback. During chlorophyll-*a* peaks (40.2 μg/L), photosynthesis elevates surface DO to supersaturation (9.1 mg/L). However, algal sedimentation/decomposition and sediment ammonia nitrogen release (bottom NH_3-N: 0.32 mg/L) intensify oxygen consumption. Although NO_3^--N shows a positive correlation with DO (r = 0.503), potentially influenced by external inputs, algal assimilation significantly reduces dissolved nitrogen concentrations. Topography-circulation coupling amplifies spatial heterogeneity. The riverine morphology (width-depth ratio: 41.7) and sluggish circulation (velocity <0.05 m/s) near the dam restrict water exchange, leading to bottom DO <0.5 mg/L in late stratification. Circulation-driven horizontal transport expands hypoxic zones, with localized hypoxia persisting even during mixing periods.

Mitigation strategies for low DO

To mitigate persistent low DO conditions, targeted management strategies were developed based on the identified synergistic mechanisms. During thermal stratification (May–September), phased flood discharge operations are recommended to destabilize thermocline formation, complemented by submersible feed delivery systems in cage-culture zones to minimize organic sedimentation and associated oxygen consumption. Concurrently, during the mixing period (November–April), selective bottom outlet discharges should be implemented to flush hypoxic water masses from the dam-front area to the Minqing Xiongjiang section (S6), combined with deep-water nanobubble-augmented aeration systems to enhance bottom-layer DO recovery rates. These stratified and zonal approaches address both seasonal hydro-thermal dynamics and site-specific hypoxia drivers in narrow-deep channel-type reservoirs.

CONCLUSIONS

This study reveals the synergistic mechanisms governing the spatiotemporal evolution of DO in narrow-deep, high-frequency disturbance channel reservoirs, exemplified by Shuikou Reservoir, and clarifies its unique dynamics distinct from typical deep reservoirs:

1) Short-term stratification-rapid mixing dynamics are key drivers of vertical DO differentiation. Riverine morphology and high-frequency flood disturbances jointly suppress stable stratification, forming a thermal stratification regime characterized by "low temperature difference and short cycle", leading to bottom hypoxia. During mixing periods, vertical DO gradients sharply decline (reduction by 79%), highlighting rapid oxygen recovery capacity.
2) Bidirectional feedback between algal metabolism and topographic circulation dominates spatial heterogeneity. Algal photosynthesis drives surface DO supersaturation (up to 9.1 mg/L), while sedimentation-driven decomposition and sediment ammonia release (NH_3-N: 0.32 mg/L) intensify bottom oxygen consumption. Coupling of sluggish dam-front circulation and topographic constraints expands hypoxic water diffusion to central zones, forming a hypoxia pattern that persists near the dam and attenuates upstream.

These findings provide a theoretical basis for DO management in high-frequency disturbance reservoirs, supporting optimization of stratification-period discharge scheduling, local oxygenation engineering in stagnant hypoxia zones, and aquaculture risk mitigation.

Acknowledgments

This work was supported by the Science and Technology Planning Project of Fujian Province ([2021R1015001] and [2021R1015002]).

REFERENCES

1. Baker, A., Scheller, M., Oriani, F., Mariethoz, G., Hartmann, A., Wang, Z., Cuthbert, M.O., (2021). Quantifying temporal variability and spatial heterogeneity in rainfall recharge thresholds in a montane karst environment. *Journal of Hydrology 594*, 125965. https://doi.org/10.1016/j.jhydrol.2021.125965
2. Caulfield, C.P., (2021). Layering, instabilities, and mixing in turbulent stratified flows. *Annual Review of Fluid Mechanics*. https://doi.org/10.1146/annurev-fluid-042320-100458
3. Çokacar, T., (2024). Cold intermediate water formation in the black sea triggered by March 2022 cold intrusions. *Journal of Marine Science and Engineering 12*, 2027. https://doi.org/10.3390/jmse12112027
4. Diaz, R.J., Rosenberg, R., (2008). Spreading dead zones and consequences for marine ecosystems. *Science 321*, 926–929. https://doi.org/10.1126/science.1156401
5. Rui, G., Suiliang, H., Yixuan, S., (2022). Vertical distribution and influencing factors of dissolved oxygen during thermal stratification in Panjiakou Reservoir. *Journal of Water Resources and Water Engineering 33*, 39–49, 57. https://doi.org/10.11705/j.issn.1672-643X.2022.03.06
6. Gorham, E., Boyce, F.M., (1989). Influence of lake surface area and depth upon thermal stratification and the depth of the summer thermocline. *Journal of Great Lakes Research 15*, 233–245. https://doi.org/10.1016/S0380-1330(89)71479-9
7. Xiaoxia, H., Guangwei, Z., Zhixu, W., (2013). Spatial-temporal variations of water quality parameters in Xin'anjiang Reservoir(Lake Qiandao) and the water protection strategy. *Lake Science 25*, 836–845.
8. Keogh, M.E., Kolker, A.S., Snedden, G.A., Renfro, A.A., (2019). Hydrodynamic controls on sediment retention in an emerging diversion-fed delta. *Geomorphology 332*, 100–111. https://doi.org/10.1016/j.geomorph.2019.02.008
9. Kraemer, B.M., Anneville, O., Chandra, S., Dix, M., Kuusisto, E., Livingstone, D.M., Rimmer, A., Schladow, S.G., Silow, E., Sitoki, L.M., Tamatamah, R., Vadeboncoeur, Y., McIntyre, P.B., (2015). Morphometry and average temperature affect lake stratification responses to climate change. *Geophysical Research Letters 42*, 4981–4988. https://doi.org/10.1002/2015GL064097
10. Lembi, C.A., (2001). Limnology, lake and river ecosystems. *Journal of Phycology 37*, 1146–1147. https://doi.org/10.1046/j.1529-8817.2001.37602.x
11. Liu, M., Zhang, Y., Shi, K., Zhu, G., Wu, Z., Liu, M., Zhang, Y., (2019). Thermal stratification dynamics in a large and deep subtropical reservoir revealed by high-frequency buoy data. *Science of The Total Environment 651*, 614–624. https://doi.org/10.1016/j.scitotenv.2018.09.215
12. Luo, Y., Zhao, Y., Yang, K., Chen, K., Pan, M., Zhou, X., (2018). Dianchi Lake watershed impervious surface area dynamics and their impact on lake water quality from 1988 to 2017. *Environ Sci Pollut Res 25*, 29643–29653. https://doi.org/10.1007/s11356-018-2967-1
13. Morgenroth, E., (2019). Editorial note. *Water Research 162*, 276. https://doi.org/10.1016/j.watres.2019.06.071
14. Nong, X., Guan, X., Chen, L., Wei, J., Li, R., (2024). Identifying environmental impacts on planktonic

algal proliferation and associated risks: a five-year observation study in Danjiangkou Reservoir, China. *Sci Rep 14*, 21568. https://doi.org/10.1038/s41598-024-70408-4

15. North, R.P., North, R.L., Livingstone, D.M., Köster, O., Kipfer, R., (2014). Long-term changes in hypoxia and soluble reactive phosphorus in the hypolimnion of a large temperate lake: consequences of a climate regime shift. *Global Change Biology 20*, 811–823. https://doi.org/10.1111/gcb.12371
16. Okkonen, J., Kløve, B., (2010). A conceptual and statistical approach for the analysis of climate impact on ground water table fluctuation patterns in cold conditions. *Journal of Hydrology 388*, 1–12. https://doi.org/10.1016/j.jhydrol.2010.02.015
17. Qiu, S., Xu, H., Long, L., Han, Y., Huang, Y., Ji, X., Song, L., Zhao, X., Yang, Z., Liu, X., Lorke, A., Ji, D., (2025). The mechanisms of hypoxia formation in a major tributary of the Three Gorges Reservoir, China. *Journal of Hydrology 658*, 133141. https://doi.org/10.1016/j.jhydrol.2025.133141
18. Slavin, E.I., Wain, D.J., Bryant, L.D., Amani, M., Perkins, R.G., Blenkinsopp, C., Simoncelli, S., Hurley, S., (2022). The effects of surface mixers on stratification, dissolved oxygen, and cyanobacteria in a shallow eutrophic reservoir. *Water Resources Research 58*, e2021WR030068. https://doi.org/10.1029/2021WR030068
19. van Heijst, G.J.F., (2014). Shallow flows: 2D or not 2D. *Environ Fluid Mech* 14, 945–956. https://doi.org/10.1007/s10652-013-9305-4
20. Winton, R.S., Calamita, E., Wehrli, B., (2019). Reviews and syntheses: Dams, water quality and tropical reservoir stratification. *Biogeosciences 16*, 1657–1671. https://doi.org/10.5194/bg-16-1657-2019
21. Wüest, A., Lorke, A., (2003). Small-scale hydrodynamics in lakes. A*nnual Review of Fluid Mechanics 35*, 373–412. https://doi.org/10.1146/annurev.fluid.35.101101.161220
22. Yan, J., Chen, N., Wang, F., Liu, Q., Wu, Z., Middelburg, J.J., Xie, Y., Guo, W., Zhang, X., (2021). Interaction between oxygen consumption and carbon dioxide emission in a Subtropical Hypoxic Reservoir, Southeastern China. *JGR Biogeosciences* 126, e2020JG006133. https://doi.org/10.1029/2020JG006133
23. Yang, K., Yu, Z., Luo, Y., Yang, Y., Zhao, L., Zhou, X., (2018). Spatial and temporal variations in the relationship between lake water surface temperatures and water quality - A case study of Dianchi Lake. *Science of The Total Environment 624*, 859–871. https://doi.org/10.1016/j.scitotenv.2017.12.119
24. Zhang, P., Liang, R.-F., Zhao, P.-X., Liu, Q.-Y., Li, Y., Wang, K.-L., Li, K.-F., Liu, Y., Wang, P., (2019). The hydraulic driving mechanisms of cyanobacteria accumulation and the effects of flow pattern on ecological restoration in Lake Dianchi Caohai. *International Journal of Environmental Research and Public Health 16*, 361. https://doi.org/10.3390/ijerph16030361
25. Zhang, P., Pang, Y., Pan, H., Shi, C., Huang, Y., Wang, J., (2015). Factors contributing to hypoxia in the Minjiang River Estuary, Southeast China. *International Journal of Environmental Research and Public Health 12*, 9357–9374. https://doi.org/10.3390/ijerph120809357
26. Zhang, P., Wang, B., Wang, Y., Pang, Y., Shi, C., Xie, R., (2022). Causes of continuous and short-term hypoxia in rivers entering the sea: a case of Minjiang River in Fujian Province. *Hydrology Research 54*, 65–81. https://doi.org/10.2166/nh.2022.095